# Calculation of high-frequency permeability of magnonic metamaterials beyond the macrospin approximation

O. Dmytriiev,[1] M. Dvornik,[1] R. V. Mikhaylovskiy,[1] M. Franchin,[2] H. Fangohr,[2] L. Giovannini,[3] F. Montoncello,[3] D. V. Berkov,[4] E. K. Semenova,[4] N. L. Gorn,[4] A. Prabhakar,[5] and V. V. Kruglyak[1,*]

[1]*School of Physics, University of Exeter, Exeter EX4 4QL, United Kingdom*

[2]*Engineering and the Environment, University of Southampton SO17 1BJ, United Kingdom*

[3]*Dipartimento di Fisica, Università di Ferrara, Via G. Saragat 1, 44122 Ferrara, Italy*

[4]*Innovent Technology Development, Pruessingstrasse, 27B, D-07745, Jena, Germany*

[5]*Indian Institute of Technology Madras, Chennai, 600036, India*

(Received 7 September 2011; revised manuscript received 11 July 2012; published 4 September 2012)

We present a method of calculation of the effective magnetic permeability of magnonic metamaterials containing arrays of magnetic inclusions of arbitrary shapes. The method fully takes into account the spectrum of spin waves confined in the inclusions. We evaluate the method by considering a particular case of a metamaterial formed by a stack of identical two-dimensional (2D) periodic hexagonal arrays of disk-shaped magnetic inclusions in a nonmagnetic matrix. Two versions of the method are considered. The first approach is based on a simple semianalytical theory that uses the numerically calculated susceptibility tensor of an isolated inclusion as input data for an analytical calculation in which the magnetodipole interaction between inclusions within each 2D array is taken into account. In the second approach, we employ micromagnetic packages with periodic boundary conditions to calculate the susceptibility of the whole 2D periodic array of such inclusions. The comparison of the two approaches reveals the necessity of retaining higher-order terms in the analytical calculation of the magnetodipole interaction via the multipole expansion. Models limited to the dipolar term can lead to remarkable underestimation of the effect of the magnetodipole interaction, in particular, for modes localized near the edge regions of inclusions. To calculate the susceptibility tensor of an isolated inclusion, we have implemented two different methods: (a) a method based on micromagnetic simulations, in which we have compared three different micromagnetic packages: the finite-element package NMAG and the two finite differences packages OOMMF and MICROMAGUS; and (b) the modified dynamical matrix method (DMM). The comparison of the different micromagnetic packages and the DMM (based on the calculation of the susceptibility tensor of an isolated inclusion) demonstrate that their results agree to within 3%. Frequency regions in which the metamaterial is characterized by the negative permeability are identified. We speculate that the proposed methodology could be generalized to more complex arrangements of magnetic inclusions, e.g., to those with multiple periods or fractal arrangements, as well as to arrays of inclusions with a distribution of properties.

DOI: 10.1103/PhysRevB.86.104405 PACS number(s): 78.67.Pt, 75.30.Ds

## I. INTRODUCTION

The recent progress in electromagnetic metamaterials has been fueled by the ability to design their unusual properties[1,2] through tweaking the geometry and structure of the constituent "meta-atoms."[3] Along with negative permittivity, negative permeability is one of the necessary features for the design of negative refractive index metamaterials. A metamaterial designer can achieve negative permeability via geometrical control of high-frequency currents, e.g., in arrays of split-ring resonators,[4] or alternatively can rely on spin resonances in natural magnetic materials,[5,6] as was suggested by Veselago in Ref. 1. However, the age of nanotechnology sets an intriguing quest for additional benefits to be gained by nanostructuring natural magnetic materials into so called *magnonic* metamaterials, in which the frequency and strength of resonances based on spin waves (magnons)[7] are determined by the geometry and magnetic configuration of meta-atoms. Spin waves can have frequencies up to hundreds of gigahertz (in the exchange-dominated regime)[6–9] and have already been shown to play an important role in the high-frequency magnetic response of composites containing magnetic inclusions of cylindrical[10–12] and spherical[13–17] shape.

The majority of analytical models for the effective permeability of magnetic composites and metamaterials employ the macrospin approximation, in which each magnetic inclusion within a nonmagnetic matrix is considered as a single giant spin and is therefore characterized by a single magnetic resonance. However, it is well known that the spin wave spectrum of magnetic nanostructures and nanoelements has a complex structure, featuring series of resonances due to spatially nonuniform spin wave modes.[18–22] Each of the resonances is expected to contribute to the susceptibility tensor of the magnetic constituents, and correspondingly to the permeability tensor of the whole metamaterial.[6,23] The resonance frequencies can be controlled and reconfigured by the external magnetic[19–25] and electric[26,27] fields, and the same functionalities could therefore be inherited by the magnonic metamaterials. Moreover, the constituent magnetic elements are extended objects and the interactions between them decay quickly with distance, so that the different magnonic resonances might be affected by the interactions differently. This circumstance increases the complexity of the observed responses and demands sophisticated theoretical methods of their description.

 

In this paper, we demonstrate a method of calculation of the effective permeability that takes full account of the complex spectrum of the metamaterial's individual magnetic constituents. The susceptibility tensor of an isolated inclusion is calculated numerically and then used as an input to an analytical expression for the permeability of the whole metamaterial. To find the susceptibility tensor of the isolated inclusion, different approaches have been used. In one of them, we have performed full-scale numerical micromagnetic simulations using three different micromagnetic packages: a finite-element based package NMAG (Ref. 28) and two finite difference based packages OOMMF (Ref. 29) and MICROMAGUS.[30] In the other approach, the dynamical matrix method, in which the system of linearized equations of motion of magnetic moments is solved to find the normal modes of a system,[31] has been modified to facilitate the susceptibility calculations. The methods have been applied to a model metamaterial representing a periodic array of magnetic nanodisks embedded within a nonmagnetic matrix. In particular, the calculations have revealed that one of the components of the effective permeability tensor of such a metamaterial becomes negative within a certain frequency range. The predictions of the method are compared with calculations based on micromagnetic simulations with the use of periodic boundary conditions (PBCs) and also with macrospin calculations. Furthermore, we use the calculations to compare the different micromagnetic methods in order to evaluate the accuracy to be expected from micromagnetic simulations. Finally, we emphasize further opportunities for generalization of the method beyond the dipolar approximation and the periodic arrangements of identical magnetic inclusions and discuss broader implications of our results on the theory of magnetostatically coupled magnetic nanostructures.

In principle, the proposed method could be considered as an extension of the concept from Ref. 6 of using magnonic resonances to tailor effective permeability of metamaterials. However, we note that the stack of thin films studied in Ref. 6 is treatable analytically. Yet, in practice, one might either want or have to deal with alternative realizations of the concept, i.e., to use magnonic meta-atoms of a different shape. For example, this could be dictated either by limitations of the available nanofabrication tools or by needs for permeability with specific frequency dependence. Such more complex magnonic metamaterials would not necessarily allow a simple analytical treatment, while numerical simulations of extended samples might present too high demands on computational resources. Our method described below circumvents the problem, to some degree in the spirit of approaches developed in Refs. 32 and 33.

## II. PERMEABILITY OF A MAGNONIC METAMATERIAL

### A. Analytical model

Let us begin by considering an idealized case of an infinitely extended three-dimensional (3D) metamaterial. To enable a meaningful introduction of the effective permeability, $\hat{\mu}$, the wavelength of electromagnetic waves should be much greater than the characteristic dimensions of the magnetic inclusions and the lattice constant of the metamaterial. Then, we can use the standard "macroscopic" relation between the high-frequency magnetic induction (**B**) and magnetic field (**H**) of the electromagnetic wave:

$$\mathbf{B} = \mathbf{H} + 4\pi\mathbf{M} = \hat{\mu}\mathbf{H}, \tag{1}$$

where **M** is the dynamic part of the magnetization that is spatially averaged over the volume of the metamaterial ("macroscopic magnetization"), and the effective permeability is defined in the frequency domain, $\hat{\mu} = \hat{\mu}(\omega)$. We generally denote macroscopic quantities by capital letters and microscopic ones by lower case ones. In particular, the static spatially averaged macroscopic magnetization is denoted as $\mathbf{M}_0$. Besides the dynamic magnetic field, **H**, there is also the external spatially uniform static magnetic field $\mathbf{H}_{\text{bias}}$.

Permeability $\hat{\mu}$ is related to macroscopic susceptibility of the whole metamaterial $\hat{\chi}$ as

$$\hat{\mu} = \hat{I} + 4\pi\hat{\chi}. \tag{2}$$

Susceptibility $\hat{\chi}$ can be found by calculating the response of the volume averaged magnetization of the metamaterial to an external uniform ac magnetic field, which in general is a complicated problem to compute. However, the problem is simplified by assuming that the metamaterial represents a lattice of magnetic elements ("inclusions") that are identical in terms of both their shape and material properties. Then, permeability $\hat{\mu}$ of the metamaterial can be related to the susceptibility of a single inclusion, $\hat{\chi}_{\text{incl}}$, via a simple equation. The problem of finding the susceptibility of a single inclusion is significantly simpler than that of finding the susceptibility of the whole metamaterial. The two susceptibilities differ due to the effect of the magnetodipole interaction between inclusions inside the metamaterial. If this interaction is absent, $\hat{\chi}$ and $\hat{\chi}_{\text{incl}}$ differ only by a factor equal to the volume fraction ("filling factor") of the magnetic inclusions in the metamaterial $\rho$ ($0 < \rho < 1$). Indeed, macroscopic magnetization **M** can be written as

$$\mathbf{M} = \rho\overline{\mathbf{m}}, \tag{3}$$

where $\overline{\mathbf{m}}$ is the dynamic "microscopic magnetization" (i.e., the one obtained via spatial averaging over the volume of a single magnetic inclusion), with the corresponding static magnetization denoted as $\overline{\mathbf{m}}_0$:

$$\overline{\mathbf{m}} = \frac{1}{V}\int\int\int_V \mathbf{m}\, dV, \tag{4}$$

where $V$ is the volume of the magnetic inclusion. The dynamic magnetization $\overline{\mathbf{m}}$ is related to the local microscopic dynamic magnetic field, $\mathbf{h}'$, through susceptibility tensor $\hat{\chi}_{\text{incl}}$, which is defined in the frequency domain as

$$\overline{\mathbf{m}} = \hat{\chi}_{\text{incl}}\mathbf{h}'. \tag{5}$$

Each magnetic inclusion by itself is characterized by a complex spectrum of spatially nonuniform spin wave modes.[18–22] Due to confinement effects, these modes can generally couple to the electromagnetic field, even if it can be considered as uniform on the scale of the inclusion's dimensions.[6] Hence, each resonant mode contributes to tensor $\hat{\chi}_{\text{incl}}$, thereby making its frequency dependence very intricate. However, micromagnetic simulations allow one to calculate $\hat{\chi}_{\text{incl}}$ of realistic inclusions of arbitrary shapes.

The macroscopic and local microscopic dynamic magnetic fields differ by the local dynamic magnetodipole field $\mathbf{h}_{\text{dyn}}$

created by the dynamic magnetization of magnetic inclusions:

$$\mathbf{h}' = \mathbf{H} + \mathbf{h}_{\rm dyn}. \tag{6}$$

Besides the dynamic magnetodipole field, $\mathbf{h}_{\rm dyn}$, there is a static magnetodipole field, $\mathbf{h}_{\rm stat}$, which is created by the static magnetization of the same inclusions. Similar to the dynamic part, local microscopic static magnetic field $\mathbf{h}_0'$ is given by

$$\mathbf{h}_0' = \mathbf{H}_{\rm bias} + \mathbf{h}_{\rm stat}. \tag{7}$$

In the considered case of the electromagnetic wavelength that is much greater than the distance between inclusions, we can express the local magnetodipole field via a tensor, $\hat{N}$, that is analogous to the tensor of demagnetizing coefficients:

$$\mathbf{h}_{\rm dyn} = -4\pi \hat{N}\overline{\mathbf{m}}. \tag{8}$$

Substituting Eqs. (2)–(8) into Eq. (1), we obtain the following general expression for effective permeability $\hat{\mu}$:

$$\hat{\mu} = \hat{I} + 4\pi\rho\hat{\chi}_{\rm incl}(\hat{I} + 4\pi\cdot\hat{N}\hat{\chi}_{\rm incl})^{-1}. \tag{9}$$

For the trivial limiting case of noninteracting inclusions, one obtains

$$\hat{\mu} = \hat{I} + 4\pi\rho\ \hat{\chi}_{\rm incl}, \tag{10}$$

as expected. We note that the latter equation also applies to the case when the interaction has been included within $\hat{\chi}_{\rm incl}$, as in some of the cases discussed below.

To illustrate the method outlined above, we evaluate the effective permeability of a metamaterial that consists of magnetic disks placed in nodes of a hexagonal lattice (Fig. 1). The distance between layers is taken to be much larger than the edge-to-edge separation between disks within each layer. Then, one can neglect the magnetodipole interaction between layers, and the metamaterial can therefore be considered as a stack of quasi-two-dimensional (2D) planes.

In the general case, dynamic magnetodipole field $\mathbf{h}_{\rm dyn}$ inside the given inclusion depends on the spatial distributions of the dynamic magnetization (mode profiles) inside all other inclusions. We can obtain $\mathbf{h}_{\rm dyn}$ using the multipole expansion method, i.e., by expanding the magnetodipole field created by each inclusion over the multipole moments of its dynamic magnetization configuration. For simplicity, in the present

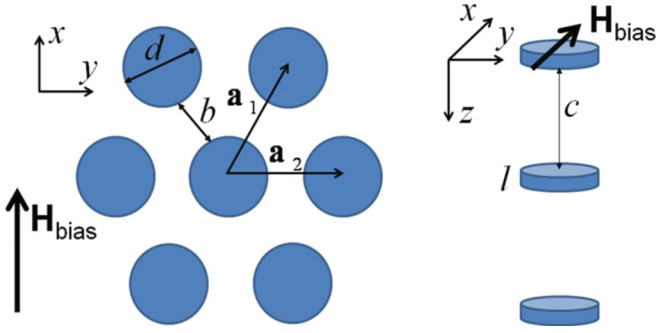


FIG. 1. (Color online) The geometry of the metamaterial consisting of magnetic disks in a nonmagnetic matrix is shown. The disks are located in nodes of a hexagonal lattice. The disk diameter is $d = 195$ nm, the in-plane edge-to-edge separation is $b = 20$ nm, and the distance between the layers is $c = 140$ nm which is much greater than disk thickness $l = 5$ nm. The filling factor is $\rho = 2.48\%$.

paper, we restrict ourselves only to the first (dipolar) term in this expansion. Then, $\mathbf{h}_{\rm dyn}$ can be expressed in terms of averaged magnetizations $\overline{\mathbf{m}}$ only as

$$\mathbf{h}_{\rm dyn} = \sum_{\mathbf{R}\neq 0} \frac{3\mathbf{R}\,(\mathbf{p}_{\rm m}\mathbf{R}) - \mathbf{p}_{\rm m}\mathbf{R}^2}{\mathbf{R}^5}, \tag{11}$$

where $\mathbf{p}_{\rm m} = \overline{\mathbf{m}}V$ is the total dynamic magnetic moment of an inclusion and the summation is performed over all nodes of one hexagonal layer. The sum in Eq. (11) converges since we perform only a 2D summation.

In the framework of the dipolar approximation, the lattice of magnetic disks is effectively replaced by the lattice of magnetic moments $\mathbf{p}_{\rm m}$ located at the centers of the disks. However, in contrast to the macrospin approximation, each magnetic moment $\mathbf{p}_{\rm m}$ here inherits the complex excitation spectrum of a single magnetic disk, both in terms of the frequencies and strength of the resonances. This approximation is valid when the energy of the interaction between disks is small enough (so that it can be considered as perturbation) and does not lead to the modification of the inclusion's ground state (i.e., for large distances between the disks). However, as the distance between the disks decreases, the profiles of some modes could be modified by the interaction, leading to significant changes in both the dynamic dipolar moments and frequencies of the modes, as observed in Ref. 34. This case requires a special consideration and shall therefore be considered in future publications.

In principle, magnetic moment $\mathbf{p}_{\rm m}$ in Eq. (11) could vary from one inclusion to another within collective magnonic modes of the metamaterial with a nonzero wave vector.[21] However, in the case of an infinitely extended metamaterial considered here, only modes with the spatial dependence following that of the incident electromagnetic wave could be excited. The frequencies of the dominant modes for a single disk are in the range of tens of gigahertz,[18,19] which corresponds to electromagnetic waves in the centimeter wavelength range. The associated spatial variation of the phase of collective magnonic modes is extremely slow and therefore can be neglected. Hence, we limit the consideration to spatially uniform excitations of the metamaterial. Then, vector $\mathbf{p}_{\rm m}$ in Eq. (11) can be taken out of the sum, and, according to definition (8), we can calculate tensor $\hat{N}$ as

$$N_{\rm ij} = -\frac{V}{4\pi}\sum_{R\neq 0}\frac{3R_{\rm i}R_{\rm j} - \delta_{\rm ij}R^2}{R^5}. \tag{12}$$

In contrast to the tensor of demagnetizing coefficients, whose trace is equal to unity, the trace of tensor $\hat{N}$ here is equal to zero, since we do not take into account the magnetic moment at the point at which we calculate the magnetic field. Instead, magnetic interactions within each magnetic inclusion are taken into account in the full micromagnetic simulations described below. To calculate tensor $\hat{N}$, we note that any lattice site of a 2D hexagonal lattice is determined by vector

$$\mathbf{R} = n_1\mathbf{a}_1 + n_2\mathbf{a}_2 = a\frac{\sqrt{3}}{2}n_2\hat{\mathbf{e}}_{\rm x} + a\left(n_1 + \tfrac{1}{2}n_2\right)\hat{\mathbf{e}}_{\rm y}, \tag{13}$$

where $a$ is the lattice period (center-to-center separation between the disks). Substituting this into Eq. (12), we calculate

$\hat{N}$ numerically to yield

$$\hat{N} = \begin{pmatrix} -\xi & 0 & 0 \\ 0 & -\xi & 0 \\ 0 & 0 & 2\xi \end{pmatrix}, \tag{14}$$

where $\xi = \frac{0.44V}{a^3}$ and the summation in Eq. (12) was performed for $n_1$,$n_2$ each ranging from $-1000$ to 1000, yielding an accuracy of $\pm 0.0001$.

In the numerical calculation of the susceptibility tensor of an isolated disk, $\hat{\chi}_{\text{incl}}$, one should take into account that, according to Eq. (7), the local static magnetic field that is experienced by each magnetic inclusion within the metamaterial and which must therefore be used in the simulations differs from external field $\mathbf{H}_{\text{bias}}$ applied to the metamaterial. The difference is equal to local static magnetodipole field $\mathbf{h}_{\text{stat}}$ originating from the other magnetic inclusions. This means that, if we simulate the susceptibility of the isolated disk for the external field $\mathbf{h}_0'$, the result obtained for the permeability of the metamaterial is valid for the applied field of

$$\mathbf{H}_{\text{bias}} = \mathbf{h}_0' - \mathbf{h}_{\text{stat}}. \tag{15}$$

The relation between the static interaction field and the static magnetization is the same as for their dynamical counterparts, so that we can follow Eq. (8) to write

$$\mathbf{h}_{\text{stat}} = -4\pi \hat{N} \overline{\mathbf{m}}_0. \tag{16}$$

### B. Macrospin approximation: Individual inclusions

In this subsection, we use the macrospin approximation to derive a simple analytical expression for susceptibility tensor $\hat{\chi}_{\text{incl}}$ and corresponding permeability tensor $\hat{\mu}$. This result is subsequently compared with susceptibility tensor $\hat{\chi}_{\text{incl}}$ calculated numerically. In the macrospin approximation, neglecting damping, the expression for $\hat{\chi}_{\text{incl}}$ follows directly from the solution of the Landau-Lifshitz equation

$$\frac{\partial \overline{\mathbf{m}}}{\partial t} = \gamma \left[\mathbf{h}_{\text{eff}} \times (\overline{\mathbf{m}}_0 + \overline{\mathbf{m}})\right], \tag{17}$$

for an isolated inclusion (a nanodisk in our case) with the effective field

$$\mathbf{h}_{\text{eff}} = \mathbf{H}_{\text{bias}} - 4\pi \hat{N}_{\text{disk}} (\overline{\mathbf{m}}_0 + \overline{\mathbf{m}}) + \mathbf{h}'(t) \tag{18}$$

where

$$\hat{N}_{\text{disk}} = \begin{pmatrix} n_{||} & 0 & 0 \\ 0 & n_{||} & 0 \\ 0 & 0 & n_{\perp} \end{pmatrix} \tag{19}$$

is the tensor of demagnetizing coefficients for an isolated disk. For thin disks, $n_{\perp} \gg n_{\parallel}$, and when the aspect ratio (thickness to radius) of a disk tends to zero (thin-film limit), we have $n_{\perp} \to 1$, $n_{\parallel} \to 0$. We find the following expression for susceptibility tensor $\hat{\chi}_{\text{incl}}$:

$$\hat{\chi}_{\text{incl}} = \begin{Bmatrix} 0 & 0 & 0 \\ 0 & \frac{\omega_M\left[\omega_{\text{H}}+(n_{\perp}-n_{||})\omega_{\text{M}}\right]}{4\pi\left(\omega_0^2-\omega^2\right)} & -\frac{i\omega_{\text{M}}\omega}{4\pi\left(\omega_0^2-\omega^2\right)} \\ 0 & \frac{i\omega_{\text{M}}\omega}{4\pi\left(\omega_0^2-\omega^2\right)} & \frac{\omega_{\text{H}}\omega_M}{4\pi\left(\omega_0^2-\omega^2\right)} \end{Bmatrix}, \tag{20}$$

where $\omega$ is the frequency of the incident electromagnetic wave, $\omega_H = \gamma H_{\text{bias}}$, $\omega_{\text{M}} = \gamma 4\pi M$, and

$$\omega_0^2 = \omega_{\text{H}}[\omega_{\text{H}} + (n_{\perp} - n_{||})\omega_{\text{M}}] \tag{21}$$

is the frequency of the uniform mode of an isolated inclusion (nanodisk). Using Eq. (9), we then find the following expression for $\hat{\mu}$:

$$\hat{\mu} = \begin{Bmatrix} 1 & 0 & 0 \\ 0 & 1 + \frac{\rho\omega_{\text{M}}\cdot\left[\omega_{\text{H}}+(n_{\perp}-n_{||}+2\xi)\omega_{\text{M}}\right]}{\Omega_{\text{dyn}}^2-\omega^2} & -\frac{i\rho\omega_{\text{M}}\omega}{\Omega_{\text{dyn}}^2-\omega^2} \\ 0 & \frac{i\rho\omega_{\text{M}}\omega}{\Omega_{\text{dyn}}^2-\omega^2} & 1 + \frac{\rho\omega_{\text{M}}\cdot(\omega_{\text{H}}-\xi\omega_{\text{M}})}{\Omega_{\text{dyn}}^2-\omega^2} \end{Bmatrix}, \tag{22}$$

where

$$\Omega_{\text{dyn}}^2 = \omega_0^2 - \xi\omega_{\text{M}}[\omega_{\text{M}}(n_{\perp} - n_{||} + 2\xi) - \omega_{\text{H}}] \tag{23}$$

is the frequency of the uniform mode of the metamaterial calculated taking into account only the internal dynamic magnetodipole field produced by the lattice of magnetic nanoparticles.

Using Eqs. (21) and (23), we can find the shift of the frequency of the uniform mode of the metamaterial with respect to the frequency of an isolated inclusion that is only due to the internal dynamic magnetodipole field produced by the lattice of magnetic inclusions:

$$\Delta\Omega_{\text{dyn}} \approx -\frac{\xi}{2} \cdot \frac{\omega_{\text{M}}[\omega_{\text{M}}(n_{\perp} - n_{||} + 2\xi) - \omega_{\text{H}}]}{\omega_0}. \tag{24}$$

This shift is negative if $(n_{\perp} - n_{||} + 2\xi)\omega_{\text{M}} > \omega_{\text{H}}$, which is usually the case for magnetic fields that are smaller than $4\pi M$.

To take into account not only the dynamic but also static magnetodipole field produced by the other inclusions within the array, we should substitute $\omega_{\text{H}}$ by $\omega_{\text{H}} + \xi\omega_{\text{M}}$ in Eqs. (22) and (23). In Eq. (22), frequency $\Omega_{\text{dyn}}$ is then replaced by the uniform resonance frequency of the metamaterial, $\Omega_0$, that takes into account both dynamic and static internal magnetodipole fields and is given by

$$\Omega_0^2 = \omega_{\text{H}}\,[\omega_{\text{H}} + (n_{\perp} - n_{||} + 3\xi)\omega_{\text{M}}]. \tag{25}$$

The total frequency shift relative to an isolated inclusion is

$$\Delta\Omega \approx \frac{3\xi}{2}\frac{\omega_{\text{M}}\omega_{\text{H}}}{\omega_0}, \tag{26}$$

i.e., is positively defined, provided that both the dynamic and static internal magnetodipole fields within the array are taken into account.

### C. Macrospin approximation: Array of inclusions

Alternatively, the same result can be obtained by applying the macrospin approximation to calculate the susceptibility of the entire 2D array of inclusions. Indeed, we have assumed that all inclusions are identical and therefore precess in phase when subject to a uniform dynamic magnetic field. This allows us to consider the dynamic magnetodipole field directly in the effective magnetic field in the Landau-Lifshitz equation

$$\begin{aligned} \mathbf{h}_{\text{eff}} &= \mathbf{H}_{\text{bias}} - 4\pi \hat{N} \overline{\mathbf{m}}_0 - 4\pi \hat{N}_{\text{disk}} (\overline{\mathbf{m}}_0 + \overline{\mathbf{m}}) + \mathbf{H}(t) - 4\pi \hat{N} \overline{\mathbf{m}} \\ &= \mathbf{H}_{\text{bias}} - 4\pi \hat{N}_{\text{tot}} (\overline{\mathbf{m}}_0 + \overline{\mathbf{m}}) + \mathbf{H}(t), \end{aligned} \tag{27}$$

where $\hat{N}_{\text{tot}} = \hat{N}_{\text{disk}} + \widehat{N}$ is the tensor of demagnetizing coefficients of the entire array, including the disk in which the magnetic field is calculated. In the limiting case of an infinite decrease of both the lattice constant, $a$, and the disk diameter, tensor $\hat{N}_{\text{tot}}$ reduces to that of a thin ferromagnetic film since tensor $\widehat{N}$ tends to zero.

Equation (27) differs from Eq. (18) only by notations. Thus, we can write for the susceptibility of the array (excluding the empty space between magnetic inclusions), $\hat{\chi}_{\text{array}}$, an expression that is analogous to Eq. (20):

$$\hat{\chi}_{\text{array}} = \begin{Bmatrix} 0 & 0 & 0 \\ 0 & \frac{\omega_M[\omega_{\text{H}}+(n_\perp-n_\parallel+3\xi)\omega_{\text{M}}]}{4\pi(\omega_0'^2-\omega^2)} & -\frac{i\omega_{\text{M}}\omega}{4\pi(\omega_0'^2-\omega^2)} \\ 0 & \frac{i\omega_{\text{M}}\omega}{4\pi(\omega_0'^2-\omega^2)} & \frac{\omega_{\text{H}}\omega_M}{4\pi(\omega_0'^2-\omega^2)} \end{Bmatrix}, \quad (28)$$

where

$$\omega_0'^2 = \omega_{\text{H}}[\omega_{\text{H}} + (n_\perp - n_\parallel + 3\xi)\omega_{\text{M}}] = \Omega_0^2. \quad (29)$$

Using Eq. (10), we then find the following expression for $\hat{\mu}$ in the macrospin approximation for the array

$$\hat{\mu} = \begin{Bmatrix} 1 & 0 & 0 \\ 0 & 1 + \frac{\rho\omega_M[\omega_{\text{H}}+(n_\perp-n_\parallel+3\xi)\omega_{\text{M}}]}{\omega_0'^2-\omega^2} & -\frac{i\rho\omega_{\text{M}}\omega}{\omega_0'^2-\omega^2} \\ 0 & \frac{i\rho\omega_{\text{M}}\omega}{\omega_0'^2-\omega^2} & 1 + \frac{\rho\omega_{\text{H}}\omega_M}{\omega_0'^2-\omega^2} \end{Bmatrix}. \quad (30)$$

Equation (30) is equivalent to Eq. (22), provided that the substitution of $\omega_{\text{H}}$ by $\omega_{\text{H}} + \xi\omega_{\text{M}}$ has been performed in the latter. The calculation described in this section is analogous to the use of PBCs in micromagnetic simulations, as discussed below (with the important difference that the dipolar interaction between inclusions is taken into account in the latter in a more rigorous way). Hence, the equivalence of the approaches used in Secs. II B and II C can also be interpreted as equivalence in the macrospin limit of the method based on the calculation of the susceptibility of a single inclusion (the main method proposed in this paper) and that based on the use of PBCs (the method that we use to test the proposed one).

## III. MICROMAGNETIC CALCULATION OF THE SUSCEPTIBILITIES OF AN ISOLATED INCLUSION AND A 2D ARRAY OF INCLUSIONS

The effective permeability of a metamaterial formed by a periodic array of magnetic inclusions can be obtained either directly from its susceptibility using Eq. (2), or from the susceptibility of an isolated inclusion using Eq. (9). From the point of view of micromagnetic calculations, the latter calculation is significantly simpler, takes less computational power, and can be performed using a greater variety of micromagnetic methods. The latter are well developed, and we will show below that the results obtained with the three particular micromagnetic codes and with the dynamic matrix method agree for our case to within 2.7%.

There are two ways to calculate the susceptibility of the whole metamaterial using micromagnetic simulations. The first one is to simulate dynamic response of a sample that is large enough to be considered as effectively infinite. In this way, one could, in principle, obtain collective magnonic excitations with all possible values of the wave vector. However, the method would require enormous computational power. The calculation of the effective permeability requires one to consider collective excitations formed by in-phase motion of meta-atoms, i.e., with the collective wave vector of zero. The response corresponding to such excitations can be calculated by a different approach. Namely, we can perform micromagnetic simulations for a relatively small array to which PBCs are applied in order to annihilate the influence of the array's edges. PBCs are realized differently in different micromagnetic packages (such as NMAG, MICROMAGUS, or OOMMF). However, the results obtained using the different packages have never been compared before. Hence, such a comparison should be carried out in order to estimate the reliability of this approach.

### A. Simulations of the susceptibility of an isolated disk

To calculate the susceptibility tensor $\hat{\chi}_{\text{incl}}$ of an isolated inclusion, we have used two different methods. In the first of them, we have performed full-scale numerical micromagnetic calculations, in which the Landau-Lifshitz-Gilbert (LLG) equation[7] is solved numerically in the time domain and the result is then Fourier transformed into the frequency domain. The second method is the dynamic matrix method (DMM), which in its initial form uses the diagonalization of the matrix computed from second derivatives of the system's energy, which is analogous to solving the linearized LLG equation.[30] In both methods, $\hat{\chi}_{\text{incl}}$ is calculated using its frequency domain definition

$$(\hat{\chi}_{\text{incl}})_{ij}(\omega) = \frac{\bar{m}_i(\omega)}{h_j'(\omega)}, \quad (31)$$

where $\bar{m}_i(\omega)$ is the Fourier transform of the $i$th component of the magnetization (spatially averaged over the volume of the inclusions) and $h_j'(\omega)$ is the Fourier transform of the $j$th component of the external dynamic magnetic field.

The geometrical and magnetic parameters used in the calculations are listed in Table I. A local magnetic field $\mathbf{h}_0'$ of 1 kOe is applied in the disk plane along the $x$ direction. From Eq. (16), the static local magnetic field for the filling factor of $\rho = 2.48\%$ is $h_{\text{stat}} = 67$ Oe. Hence, the calculation corresponds to the external magnetic bias field applied to the metamaterial $H_{\text{bias}} = 933$ Oe.

#### 1. Micromagnetic simulations

In simulations performed by all packages the disk-shaped nanoelement was excited by a short transient magnetic field of the same temporal form, and the instantaneous spatially

TABLE I. The geometrical and magnetic parameters used in the calculations are listed.

| Parameter | Value |
|---|---|
| Disk diameter ($d$) | 195 nm |
| Disk thickness ($l$) | 5 nm |
| Saturation magnetization ($M$) | 800 G |
| Exchange constant ($A$) | 1.3 $\mu$erg/cm |
| Gilbert damping constant ($\alpha$) | 0.01 |
| Gyromagnetic ratio ($\gamma$) | $2\pi \times 2.8$ GHz/kOe |

averaged magnetization was recorded every 10 ps over the time interval of 10.24 ns. However, the discretization cell size was different in simulations performed using different packages. In OOMMF, a uniform discretization into cells with dimensions of $1 \times 1 \times 5$ nm$^3$ was used, without the use of the edge correction algorithm. In MICROMAGUS, the cell size was $2 \times 2 \times 5$ nm$^3$, while the magnetization of the edge cells was additionally reduced according to the volume fraction of the cells within a circle of the nanodisk radius. We note in passing that this procedure is different from the gradual reduction of the edge cell magnetization towards the element edge applied in Ref. 35. The latter procedure leads to a reduction of magnetic charges at and associated reduction of the demagnetizing field near the edges perpendicular to the applied magnetic field, thereby increasing the edge mode frequency.[35,36] The main effect of the magnetization reduction used in MICROMAGUS (which is applied only to those cells which are crossed by the curved element boundary) is a more adequate representation of the nanodisk border. Due to the ability of the finite-element packages to use site-dependent meshes, in NMAG we could use an irregular mesh: small elements with the size of ∼0.5 nm near the edges and larger elements with the typical sizes of ∼2 nm at the center of the disk. It was also checked that further decrease of the cell size did not lead to significant changes in the calculated susceptibility.

To solve the LLG equation, in MICROMAGUS we have used the Bogacki-Shampine version of the Runge-Kutta-23 method, which enables the integration step size control to achieve the required dynamical accuracy (in our case, we have set the accuracy to $10^{-6}$ and checked that further accuracy improvement did not change the final result). In NMAG, we have used the second-order backward differentiation formula (BDF) as implemented by the SUNDIALS package.[37] The preconditioned Newton method is used to solve the implicit formula (these are the default settings in NMAG).

The excitation field $\mathbf{h}_0'$ was taken in the form of the "sinc" function and applied along corresponding coordinate axes, in order to obtain various components of $\hat{\chi}_{\text{incl}}$:

$$\mathbf{h}' = h_{\max} \frac{\sin\left[2\pi f_0 (t - t_0)\right]}{2\pi f_0 (t - t_0)}, \tag{32}$$

where amplitude $h_{\max}$ is 10 Oe, cut-off frequency $f_0$ is 30 GHz, and $t_0 = 10/2f_0$ ns. The pulse form given by Eq. (32) has a constant power spectrum up to cut-off frequency $f_0$. This feature assures that all system eigenmodes with frequencies $f < f_0$ are excited with an approximately constant "strength."

### 2. *Modified dynamical matrix method*

The dynamical matrix method allows one to study spin wave modes of a magnetic particle of arbitrary shape and nonuniform equilibrium magnetization state, taking into account the external field, magnetic anisotropies, and the magnetodipole and exchange interactions.[31] In the present work, the original version of the method has been modified by including two additional terms: an external magnetic excitation at fixed frequency and the Gilbert damping. Thereby, the mathematical problem is changed from a generalized eigenvalue problem to a nonhomogeneous linear system. Assuming that the magnetic particle is discretized into $N$ identical interacting cells, and that the uniform normalized magnetization in each cell $\mathbf{m}_i$ is represented by polar and azimuthal angles $\theta_i$ and $\varphi_i$, the equations of motion in the linear regime in the frequency domain become

$$\left(\hat{H} + \frac{\mathrm{M_S}\omega}{\gamma}\hat{A}\right)\mathbf{v} = \mathrm{M_S}\mathbf{w}, \tag{33}$$

where $\hat{H}$ is the Hessian matrix of the system, i.e., the matrix of second partial derivatives of the energy calculated in the ground state. Matrix $\hat{A}$ is given by

$$\hat{A} = \begin{pmatrix} i\alpha \sin^2\varphi_1 & -i\sin\varphi_1 & 0 & 0 & \cdots \\ i\sin\varphi_1 & i\alpha & 0 & 0 & \cdots \\ 0 & 0 & i\alpha\sin^2\varphi_2 & -i\sin\varphi_2 & \cdots \\ 0 & 0 & i\sin\varphi_2 & i\alpha & \cdots \\ \cdots & \cdots & \cdots & \cdots & \cdots \end{pmatrix}, \tag{34}$$

$\mathbf{v}$ is the vector of the magnetization fluctuations (variables),

$$\mathbf{v} = \begin{pmatrix} \delta\theta_1 \\ \delta\varphi_1 \\ \vdots \\ \delta\theta_{\mathrm{N}} \\ \delta\varphi_{\mathrm{N}} \end{pmatrix}, \tag{35}$$

and vector $\mathbf{w}$ in the right-hand side is

$$\mathbf{w} = \begin{pmatrix} \mathbf{h}' \cdot \frac{\partial \mathbf{m}_1}{\partial \theta_1} \\ \mathbf{h}' \cdot \frac{\partial \mathbf{m}_1}{\partial \varphi_1} \\ \vdots \\ \mathbf{h}' \cdot \frac{\partial \mathbf{m}_1}{\partial \theta_{\mathrm{N}}} \\ \mathbf{h}' \cdot \frac{\partial \mathbf{m}_1}{\partial \varphi_{\mathrm{N}}} \end{pmatrix}. \tag{36}$$

The new terms with respect to the original formulation (Ref. 31) are the nonhomogeneous term $\mathbf{w}$ and the diagonal elements in $\hat{A}$. Here, $\mathbf{h}'$ is the homogeneous external field oscillating at frequency $\omega$ as discussed above. The linear system of Eq. (33) can be solved for any frequency, and corresponding average magnetization $\overline{\mathbf{m}} = \mathrm{M_S}\sum_i \mathbf{m}_i/N$ is then used to find the susceptibility defined by Eq. (31).

For the numerical solution of Eq. (33), we used an iterative method. Finding the solution of a large, complex, non-Hermitian system of linear algebraic equations is a difficult task, especially close to singular points, corresponding to frequencies of self-oscillations of the magnetic particle. An iterative method allows one to use the result obtained at a given frequency as the initial value for the search of the solution at the next frequency, thereby reducing the convergence time. We have chosen the biconjugate gradient squared method with stabilization.[38] This method refers the matrix of the system only through its multiplication by a vector, or the multiplication of its transpose conjugate by a vector, so that we can easily exploit the symmetries of matrices $\hat{H}$ (real, symmetric) and $\hat{A}$ (sparse, tridiagonal) for an efficient implementation of the algorithm.

The susceptibility of the isolated disk-shaped nanoelement has been calculated using a uniform discretization into cells

with dimensions of $3 \times 3 \times 5$ nm$^3$. Albeit larger than that used for the other methods, this cell size allows us to reduce the number of independent variables in the numerical problem to a manageable size. In fact, despite the unquestionable advantages of the iterative method chosen for solving the complex system of equations, its convergence is not guaranteed, in particular failing when the number of variables is too large.

### B. Micromagnetic simulations using periodic boundary conditions

To calculate the susceptibility tensor $\hat{\chi}$ from simulations with PBCs, we have used two micromagnetic codes: NMAG and MICROMAGUS. We have performed the simulations with the unit cell of two magnetic disks and PBCs. PBCs are realized differently in different micromagnetic packages. The underlying aim is, however, always the same: to reduce the effect of the finite size, i.e., by modifying the internal field in a finite array so that the array can be treated as a part of an infinite one. The susceptibility $\hat{\chi}$ is again calculated using Eq. (31).

In NMAG, PBCs are realized through the possibility to create a finite number of virtual copies of the simulated object[39] (two disks in our case). The magnetization dynamics in every virtual copy repeats the one in the simulated object. The magnetization dynamics in the simulated object is simulated taking into account both static and dynamic magnetodipole fields produced by the virtual copies. In the NMAG simulations reported here, we created as many virtual copies as was necessary to obtain a virtual array of $7 \times 5$ disks, which corresponds to the virtual sample size of $\sim 1.5 \times 1.7$ $\mu$m$^2$. Furthermore, we have checked that a further increase of the size of the virtual array to $11 \times 7$ or $\sim 2.3 \times 2.4$ $\mu$m$^2$ leads only to an insignificant increase of the frequency by 0.016 GHz.

In MICROMAGUS, PBCs are taken into account using the rigorous Ewald method for the magnetodipole interaction, developed by the package authors initially for a 2D lattice of point dipoles[40] and extended later to the case of a system discretization by finite rectangular prisms.[41] For this reason, the simulation area used by MICROMAGUS includes only one elementary lattice cell of two nanodisks.

## IV. RESULTS AND DISCUSSION

In Fig. 2, four components of the permeability tensor of the metamaterial calculated using Eq. (9) are presented. The blue solid lines, dashed red lines, green open dots, and black filled dots show the permeability calculated using OOMMF, NMAG, MICROMAGUS, and DMM, respectively. For the in-plane edge-to-edge separation $b = 20$ nm assumed in the calculations and the interlayer distance $c = 140$ nm, the filling factor of the magnetic material is $\rho = 2.48\%$. One can clearly see the contributions from the two main resonances of the nanodisk (meta-atoms) into the effective permeability tensor of the metamaterial. The first (lower frequency) resonance corresponds to the edge mode.[36] This mode does not have nodal lines. The second resonance corresponds to the first bulk mode with two nodal lines perpendicular to the direction of the bias field. The bias magnetic field of $H_{\text{bias}} = 933$ Oe is applied in the plane of the metamaterial layers along the $x$ axis

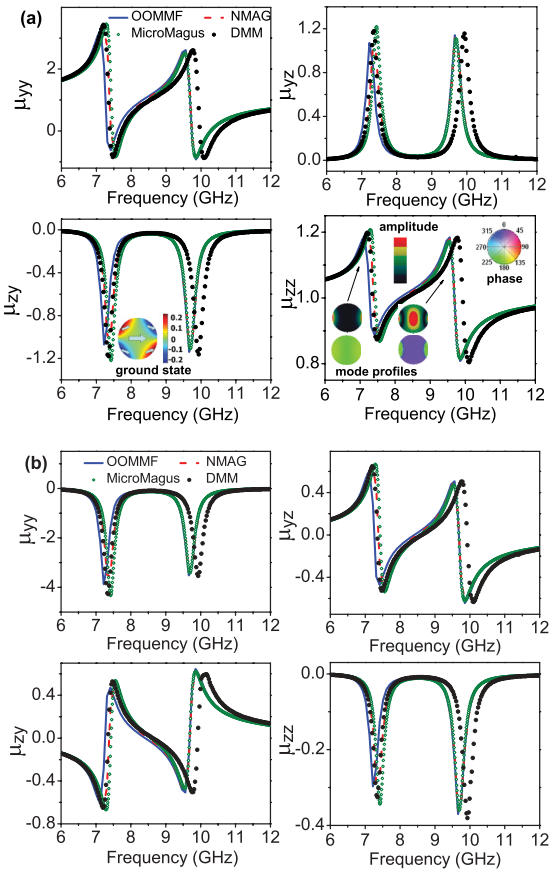


FIG. 2. (Color online) The real (a) and imaginary (b) parts of four components of effective permeability tensor $\mu$ calculated using Eq. (9) are shown as functions of the frequency for the metamaterial depicted in Fig. 1. External magnetic field $H_{\text{bias}} = 933$ Oe is applied in the plane of the layers along the horizontal line. The blue solid lines, dashed red lines, green open dots, and black filled dots show the permeability calculated using OOMMF, NMAG, MICROMAGUS, and DMM, respectively. The insets show the distribution of the normalized magnetization component orthogonal to the applied field in the ground state in a single nanodisk; the spatial profiles of the mode amplitude (top) and phase (bottom) for the two dominant modes of a single nanodisk.

(i.e., horizontally) in Fig. 2 with the mode profiles[42] shown in the insets of the figure. The inset also shows the distribution of the normalized magnetization component orthogonal to the applied field in the ground state in the single nanodisk. This picture shows that the applied field is sufficiently large to achieve an almost saturated equilibrium magnetization state of the sample. For this reason, the real part of the $xx$ component of the effective permeability differs insignificantly from unity and the $xy$, $yx$, $xz$, and $zx$ components are almost zero, with the latter differences being due to small ground state nonuniformities caused by the strong demagnetizing field near the edges of metamaterial constituents. Hence, these components are not displayed in Fig. 2. The $yy$ and $zz$ components differ in magnitude by more than seven times. This difference is due to the ellipticity of the precession (caused by the demagnetizing field of the thin nanodisk), with the in-plane oscillation amplitude being much greater than that of the out-of-plane oscillation. When studying metamaterials,

TABLE II. The resonant frequencies of the two dominant modes of an isolated nanodisk obtained by different micromagnetic packages and the DMM.

| Package | Edge mode (GHz) | Bulk mode (GHz) |
|---|---|---|
| OOMMF | 7.35 | 9.82 |
| NMAG | 7.49 | 9.83 |
| MICROMAGUS | 7.55 | 9.82 |
| DMM | 7.46 | 10.05 |

frequency domains in which negative values of the effective permeability can be achieved are especially important, due to the possibility of realizing negative refraction.[6] As shown in Fig. 2, the $yy$ component of the effective permeability becomes negative near both resonant frequencies at the particular value of the filling factor.

As one can see from Fig. 2, all three micromagnetic packages and the DMM yield very similar results for the frequency dependence of the permeability tensor components. To compare the results given by the different methods quantitatively, Table II summarizes the frequencies of the permeability resonances corresponding to the two dominant modes of the corresponding isolated nanodisk (meta-atom). For the edge mode (the lowest-frequency mode), the greatest discrepancy is observed between predictions of OOMMF and MICROMAGUS, with the difference of 0.2 GHz or about 2.7% of the average edge mode frequency. The difference is most likely to result from the different discretization methods of the disk edges used in the calculations by the different packages. Indeed, the edge mode is strongly localized near the disk edges, where the internal magnetic field varies significantly over distances of a couple of nanometers from the edges. So, the discretization method and the treatment of the magnetodipole field created by the edge cells play an important role for the edge mode.[43] In particular, we found that for the studied sample the frequency of the edge mode decreased in NMAG, increased in OOMMF, and remained nearly constant in MICROMAGUS as the cell size of the underlying mesh decreased. In NMAG and OOMMF, we have checked that a decrease of the cell size beyond that used in the calculations reported here does not lead to significant changes in the calculated resonant frequencies.

For the bulk mode (the higher-frequency mode), all three micromagnetic packages give identical predictions. This result is expected, because the mode occupies predominantly the inner region of the disk, so that the details of the edge discretization play a minor role. The DMM predicts a value that is 0.23 GHz (or about 2.3% of the average bulk mode frequency) larger than that predicted by the micromagnetic packages. The difference is probably due to the larger cell size used in the DMM calculations, which makes the representation of the mode with oscillations less accurate. The iterative algorithm used in this case for solving the general, complex, linear system involved in the DMM may also have a role, introducing numerical errors (for this algorithm an error around 1% is quite possible). More information on the influence of the mesh sizes on different modes in confined magnetic elements can be found, e.g., in Ref. 43.

The resonant frequencies in the permeability of the metamaterial are shifted by about $\Delta\Omega \approx 0.17$ GHz relative to those of the corresponding spin wave modes of an isolated nanodisk. As discussed for the macrospin calculations, the shift contains two competing contributions of the dynamic and static magnetodipole fields. The contribution from the dynamic fields is negative and has been estimated by a straight application of Eq. (9) to the susceptibility of the nanodisk, as about $\Delta\Omega_{\text{dyn}} \approx -0.12$ GHz, varying insignificantly for the different modes and packages. The effect of the increase of the static internal field by 67 Oe has been estimated by calculating the mode frequencies for an isolated nanodisk at $H_{\text{bias}} =$ 933 Oe and 1 kOe, to result in an increase of the frequency by about $\Delta\Omega_{\text{stat}} = 0.29$ GHz. Therefore, dynamic and static magnetodipole fields within the array lead to frequency shifts of opposite signs, and together they lead to the observed net increase of the resonant frequencies of the metamaterial of about 0.17 GHz.

Let us compare the results of the full micromagnetic calculations and those obtained using the macrospin approximation. The frequency of the only resonance predicted for the metamaterial by the macrospin model is calculated using Eq. (25) and the parameter values given in Table I to yield $\Omega_0 = 9.02$ GHz. The value is about 1 GHz lower and about 1.5 GHz higher than the frequencies of the bulk and edge modes, respectively, as obtained from the micromagnetic calculations. Furthermore, the macrospin model predicts a total shift [Eq. (26)] of $\Delta\Omega \approx 0.08$ GHz, which includes a contribution due to the dynamic magnetodipole field [Eq. (24)] of $\Delta\Omega_{\text{dyn}} \approx -0.27$ GHz. Perhaps expectedly, the results demonstrate the failure of the macrospin approximation to predict the microwave permeability and, more generally, dynamic magnetic properties of magnonic metamaterials composed of nonellipsoidal magnetic inclusions. In contrast, the proposed method based on full micromagnetic calculations allows us to take into account contributions of all eigenmodes of constituent magnetic inclusions of a nonellipsoidal shape to the effective permeability. Yet, the semianalytical nature of the micromagnetic model allows us to compare the contributions of dynamic and static magnetodipole fields to the observed frequency dependence of the permeability.

Figure 3 shows the $zz$ component of the effective permeability tensor calculated from Eq. (10) with the susceptibility tensor calculated from micromagnetic simulations performed using PBCs as explained in Sec. III B. For comparison, we also show the permeability of the metamaterial consisting of noninteracting magnetic disks based on the susceptibility of a single disk calculated by NMAG and MICROMAGUS, respectively. Thereby Fig. 3 demonstrates the effect of the interaction between metamaterial constituents on the resonant modes of the metamaterial. Table III shows the frequency shifts of the dominant modes of the metamaterial calculated using Eqs. (9) and (10) with respect to the frequencies of the corresponding modes of an isolated nanodisk (open boundary conditions). The frequency shifts predicted by the two packages in simulations with PBCs [Eq. (10)] differ by 0.04 GHz for the edge mode and 0.1 GHz for the bulk mode, while the application of Eq. (9) to the simulation results for an isolated disk yielded nearly identical values for the bulk mode and a difference of 0.03 GHz for the frequency of the edge mode. The difference between the two micromagnetic packages in simulations with PBCs is insignificant given the

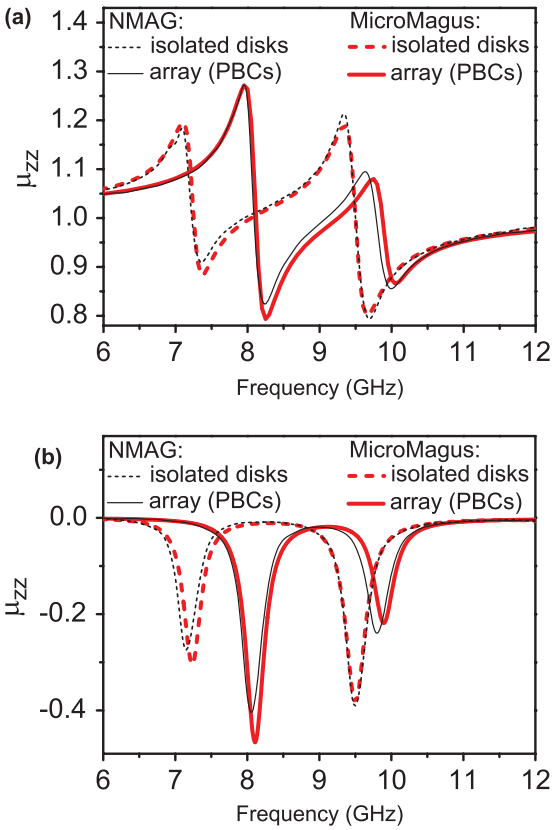


FIG. 3. (Color online) The real (a) and imaginary (b) parts of the $zz$ component of the effective permeability tensor calculated using Eq. (10) with the susceptibility tensor calculated from micromagnetic simulations with PBCs are shown as functions of the frequency for the metamaterial depicted in Fig. 1. External magnetic field $H_{\text{bias}} =$ 933 Oe is applied in the plane of the layers parallel to the $x$ axis. The thin black and thick red dashed lines show the permeability of the metamaterial consisting of noninteracting magnetic disks based on the susceptibility of a single disk calculated by NMAG and MICROMAGUS, respectively. The thin black and thick red solid lines show the permeability of the metamaterial calculated using PBCs by NMAG and MICROMAGUS, respectively.

discrepancy of 0.06 GHz and <0.01 GHz in predictions of the same two packages for the edge and bulk modes of an isolated disk, respectively, and can be still attributed to the same reason as for an isolated disk, i.e., to the different methods of the edge discretization. The relatively large difference between the bulk mode frequencies in simulations with PBC performed by NMAG and MICROMAGUS can be only due to different algorithms of the PBC realization in these packages.

TABLE III. The frequency shifts for the dominant modes of the metamaterial with respect to those of an isolated nanodisk as calculated using the approximate method [i.e., Eq. (9)] and the simulations with PBCs [Eq. (10)], for NMAG and MICROMAGUS.

| | Edge mode (GHz) | | Bulk mode (GHz) | |
|---|---|---|---|---|
| Package | Equation (9) | Equation (10) | Equation (9) | Equation (10) |
| NMAG | 0.22 | 0.91 | 0.2 | 0.3 |
| MICROMAGUS | 0.19 | 0.87 | 0.2 | 0.4 |

The shift of the lower metamaterial resonant frequency with respect to the edge mode of an isolated nanodisk predicted by the micromagnetic simulations with PBCs is significantly larger than that in the proposed semianalytical method. At the same time, the micromagnetic simulations with PBC predict a shift of the higher metamaterial resonant frequency with respect to the bulk mode of a nanodisk that is again larger than and yet comparable with that in the semianalytical method. This can be explained by the fact that the bulk mode is localized in the inner part of the disk where the magnetodipole field produced by the other disks in the metamaterial is described reasonably well by the dipolar approximation used in the calculations. An important broader consequence of this analysis is that the dipolar approximation might fail for phenomena in which the edge mode plays a significant role. The results might therefore question some of the previous dipole-only theoretical studies of magnetostatically coupled magnetic nanostructures, not only in the context of metamaterials but also of magnonic dispersion relations for arrays of magnetic elements and perhaps dynamic response of closely packed magnetic random access memory (MRAM) cells or bit-patterned media.

In the studied example, we considered a metamaterial with a periodic arrangement of identical magnetic inclusions. This allowed us to simplify the calculations significantly, firstly, in the summation in Eq. (12), and secondly, since the micromagnetic simulations for the inclusion had to be performed at a single value of the applied magnetic field and for a single set of magnetic parameters. At the same time, magnonic metamaterials with more complex arrangements[44–47] of magnetic inclusions could also prove interesting from both applied and fundamental points of view. In principle, the methodology presented in this paper could be extended to such arrangements as well as to systems with variation of the inclusions' properties (including, e.g., systems with defect states[48,49]) and with other (e.g., nondipolar) forms of coupling between inclusions.[50–52] Such extensions are, however beyond, the scope of the present study, which aims mainly to demonstrate the strength and versatility of combining the (more accurate) full micromagnetic simulations with lattice calculations.

## V. CONCLUSIONS

We have shown that full micromagnetic simulations and calculations based on the dynamical matrix method provide a useful complementary tool to the well-developed averaging procedures widely used in the theory of the effective permeability of metamaterials. For the model case of a periodic array of ferromagnetic disks in a nonmagnetic matrix, we have been able to calculate the effective permeability tensor taking into account all resonances of the metamaterial constituents. We have compared the proposed suggested model with that based on the macrospin approximation and with the direct permeability calculation based on micromagnetic simulations with periodic boundary conditions. We show that the effective permeability of the studied metamaterial can reach negative values in the vicinity of the magnonic resonances in the low-gigahertz range. However, higher frequencies should be readily available if a more sophisticated magnetic nanoengineering is

used. Such systems will still be treatable within the proposed formalism and are a subject of future studies. We also note that the observed complexity of the magnetic response of magnonic metamaterials is specific to the high-frequency permeability resulting from micromagnetics of magnetic nanoelements. This complexity represents an interesting development for the theory of metamaterials and the nanomagnetism, the latter in particular including magnonics.

The presented calculation also provides a useful method by which to evaluate the accuracy of the different micromagnetic packages and the dynamical matrix method, in both the frequency and amplitude of the response. In particular, we find that the results produced by the state-of-the-art micromagnetic simulations agree with each other within an error bar of about 3%, which has to be taken into account when micromagnetic calculations are used to model experimental data. Finally, our calculations demonstrate that in order to reproduce correctly the magnetodipole interaction between elements within the studied array one has to take into account higher-order multipole magnetic moments of the constituent magnetic elements. Our analyses reveal that the interaction due to the higher terms could be particularly important for a correct description of dynamic phenomena mediated by magnonic modes localized near the edges of the inclusions, with far-going consequences beyond the theory of the effective permeability of magnonic metamaterials and more generally magnonics.

## ACKNOWLEDGMENTS

The research leading to these results has received funding from the ECs 7th Framework Programme (FP7/2007-2013) under Grant Agreements No. 228673 (MAGNONICS) and No. 233552 (DYNAMAG) and from EPSRC of the UK under Project No. EP/E055087/1.

*V.V.Kruglyak@exeter.ac.uk

[1] V. G. Veselago, Sov. Phys. Usp. **10**, 509 (1968).
[2] J. B. Pendry, D. Schurig, and D. R. Smith, Science **312**, 1780 (2006).
[3] J. B. Pendry, Phys. Rev. Lett. **85**, 3966 (2000).
[4] J. B. Pendry, A. J. Holden, D. J. Robbins, and W. J. Stewart, IEEE Trans. Microwave Theory Tech. **47**, 2075 (1999).
[5] O. Acher, J. Magn. Magn. Mater. **321**, 2093 (2009).
[6] R. V. Mikhaylovskiy, E. Hendry, and V. V. Kruglyak, Phys. Rev. B **82**, 195446 (2010).
[7] A. G. Gurevich and G. A. Melkov, *Magnetization Oscillations and Waves* (CRC Press, Boca Raton, FL, 1996).
[8] M. Dvornik, A. N. Kuchko, and V. V. Kruglyak, J. Appl. Phys. **109**, 07D350 (2011).
[9] V. V. Kruglyak, S. O. Demokritov, and D. Grundler, J. Phys. D: Appl. Phys. **43**, 264001 (2010).
[10] U. Ebels, J. L. Duvail, P. E. Wigen, L. Piraux, L. D. Buda, and K. Ounadjela, Phys. Rev. B **64**, 144421 (2001).
[11] G. S. Makeeva, M. Pardavi-Horvath, and O. A. Golovanov, IEEE Trans. Magn. **45**, 4074 (2009).
[12] V. Boucher, L.-P. Carignan, T. Kodera, C. Caloz, A. Yelon, and D. Ménard, Phys. Rev. B **80**, 224402 (2009).
[13] S. Rajagopalan and J. K. Furdyna, Phys. Rev. B **39**, 2532 (1989).
[14] A. Aharoni, J. Appl. Phys. **69**, 7762 (1991); **81**, 830 (1997).
[15] G. Viau, F. Fievet-Vincent, F. Fievet, P. Toneguzzo, F. Ravel, and O. Acher, J. Appl. Phys. **81**, 2749 (1997).
[16] D. Mercier, J.-C. S. Levy, G. Viau, F. Fievet-Vincent, F. Fievet, P. Toneguzzo, and O. Acher, Phys. Rev. B **62**, 532 (2000).
[17] J. Ramprecht and D. Sjöberg, J. Phys. D: Appl. Phys. **41**, 135005 (2008).
[18] R. D. McMichael and M. D. Stiles, J. Appl. Phys. **97**, 10J901 (2005).
[19] V. V. Kruglyak, P. S. Keatley, A. Neudert, M. Delchini, R. J. Hicken, J. R. Childress, and J. A. Katine, Phys. Rev. B **77**, 172407 (2008).
[20] F. Montoncello, L. Giovannini, F. Nizzoli, H. Tanigawa, T. Ono, G. Gubbiotti, M. Madami, S. Tacchi, and G. Carlotti, Phys. Rev. B **78**, 104421 (2008).
[21] V. V. Kruglyak, P. S. Keatley, A. Neudert, R. J. Hicken, J. R. Childress, and J. A. Katine, Phys. Rev. Lett. **104**, 027201 (2010).
[22] J. Topp, D. Heitmann, M. P. Kostylev, and D. Grundler, Phys. Rev. Lett. **104**, 207205 (2010).
[23] M. Mruczkiewicz, M. Krawczyk, R. V. Mikhaylovskiy, and V. V. Kruglyak, Phys. Rev. B **86**, 024425 (2012).
[24] E. J. Kim, J. L. R. Watts, B. Harteneck, A. Scholl, A. Young, A. Doran, and Y. Suzuki, J. Appl. Phys. **109**, 07D712 (2011).
[25] V. L. Zhang, Z. K. Wang, H. S. Lim, S. C. Ng, M. H. Kuok, S. Jain, and A. O. Adeyeye, J. Nanosci. Nanotechnol. **11**, 2657 (2011).
[26] P. Rovillain, R. de Sousa, Y. Gallais, A. Sacuto, M. A. Measson, D. Colson, A. Forget, M. Bibes, M. Barthelemy, and M. Cazayous, Nat. Mater. **9**, 975 (2010).
[27] A. Kumar, J. F. Scott, and R. S. Katiyar, Appl. Phys. Lett. **99**, 062504 (2011).
[28] T. Fischbacher, M. Franchin, G. Bordignon, and H. Fangohr, IEEE Trans. Magn. **43**, 2896 (2007); http://NMAG.soton.ac.uk.
[29] M. Donahue and D. G. Porter, OOMMF User's Guide, Version 1.0, Interagency Report No. NISTIR 6376, NIST, 1999; http://math.nist.gov/oommf.
[30] D. V. Berkov and N. L. Gorn, MICROMAGUS package for micromagnetic simulations, http://www.micromagus.de.
[31] M. Grimsditch, L. Giovannini, F. Montoncello, F. Nizzoli, G. K. Leaf, and H. G. Kaper, Phys. Rev. B **70**, 054409 (2004).
[32] L. Giovannini, F. Montoncello, and F. Nizzoli, Phys Rev. B **75**, 024416 (2007).
[33] K. Rivkin, W. Saslow, V. Chandrasehkhar, L. E. De Long, and J. B. Ketterson, Phys Rev. B **75**, 174408 (2007).
[34] M. Dvornik, P. V. Bondarenko, B. A. Ivanov, and V. V. Kruglyak, J. Appl. Phys. **109**, 07B912 (2011).
[35] R. D. McMichael and B. B. Maranville, Phys. Rev. B **74**, 024424 (2006).
[36] V. V. Kruglyak, A. Barman, R. J. Hicken, J. R. Childress, and J. A. Katine, Phys. Rev. B **71**, 220409 (2005).
[37] https://computation.llnl.gov/casc/sundials/documentation/cv_guide.pdf.
[38] H. A. van der Vorst, SIAM J. Sci. Stat. Comput. **13**, 631 (1992).
[39] H. Fangohr, G. Bordignon, M. Franchin, A. Knittel, P. A. J. de Groot, and T. Fischbacher, J. Appl. Phys. **105**, 07D529 (2009).

[40]D. V. Berkov and N. L. Gorn, Phys. Rev. B **57**, 14332 (1998).
[41]D. V. Berkov and N. L. Gorn, IEEE Trans. Magn. **38**, 2474 (2002).
[42]The mode profiles were calculated using SEMARGL, http://www.magnonics.org/semargl/; M. Dvornik and V. V. Kruglyak, Phys. Rev. B **84**, 140405 (2011).
[43]R. E. Camley, B. V. McGrath, Y. Khivintsev, Z. Celinski, R. Adam, C. M. Schneider, and M. Grimsditch, Phys. Rev. B **78**, 024425 (2008).
[44]V. A. Ignatchenko, Y. I. Mankov, and D. S. Tsikalov, J. Exp. Theor. Phys. **107**, 603 (2008).
[45]I. P. Coelho, M. S. Vasconcelos, and C. G. Bezerra, Solid State Commun. **150**, 1760 (2010).
[46]J. Ding, M. Kostylev, and A. O. Adeyeye, Phys. Rev. Lett. **107**, 047205 (2011).
[47]I. P. Coelho, M. S. Vasconcelos, and C. G. Bezerra, J. Magn. Magn. Mater. **323**, 3162 (2011).
[48]A. N. Kuchko, M. L. Sokolovskii, and V. V. Kruglyak, Physica B **370**, 73 (2005).
[49]H. Yang, G. H. Yun, and Y. J. Cao, J. Appl. Phys. **111**, 013908 (2012).
[50]M. Krawczyk, J. Klos, M. L. Sokolovskyy, and S. Mamica, J. Appl. Phys. **108**, 093909 (2010).
[51]S. L. Vysotskii, S. A. Nikitov, E. S. Pavlov, and Y. A. Filimonov, J. Commun. Technol. Electron. **55**, 800 (2010).
[52]R. S. Iskhakov, S. V. Stolyar, M. V. Chizhik, and L. A. Chekanova, JETP Lett. **94**, 301 (2011).